ANTISOLVENT PRECIPITATION: INTERACTION OF MIXING, PHASE BEHAVIOUR, AND PARTICLE FORMATION

A. Braeuer[1]*, S. Dowy[1], R. Schatz[2], E. Schluecker[2] and A. Leipertz[1].
[1]*Lehrstuhl für Technische Thermodynamik and Erlangen Graduate School in Advanced Optical Technologies (SAOT), Universität Erlangen-Nürnberg, Am Weichselgarten 8, 91058 Erlangen, Germany*
[2]*Lehrstuhl für Prozessmaschinen und Anlagentechnik, Universität Erlangen-Nürnberg, Cauerstrasse 4, 91058 Erlangen, Germany*
ab@ltt.uni-erlangen.de & 0049 9131 8525853

In this report we give a review on a variety of optical measurements, we carried out in situ to analyze the supercritical antisolvent particle precipitation. The measurement techniques comprise shadography, Mie scattering and Raman scattering. These measurement techniques provide mole fraction distributions, antisolvent partial density distributions, distribution of the precipitated particles and progress of mixing distributions. The information extractable from these measurements cover time scales for mixing and precipitation, flow fields, supersaturation which causes precipitation, and how the precipitated particles affect the mixing mechanisms. The experiments were carried out in the system paracetamol, ethanol and CO_2.

INTRODUCTION

Supercritical antisolvent atomization is a suitable method for the production of fine powders as important particle properties such as size, size distribution and morphology can be adjusted by varying process parameters like the solute concentration, the solvent/antisolvent-ratio and the operation conditions like pressure and temperature [1]. From a variety of action-reaction experiments Reverchon et al. [2, 3] extracted a model which puts the process parameters and the resulting particle properties into relation. This model is based onto the phase behaviour of the pseudo (without solute) binary mixture of solvent and antisolvent and allows the targeted production of particles for many SAS-systems. Whenever the presence of solute affects the binary phase behaviour –as it is the case for the system paracetamol, ethanol and CO_2-, this model fails. Thus to understand why, we analyzed the intermediate mechanisms between the set process parameters and the resulting particles. This is exactly that part of the SAS-precipitation not considered in the mentioned model. To learn about these intermediate steps inside the SAS-precipitation chamber, we carried out different in-situ optical experiments. In this manuscript we summarize our optical investigations and provide the respective conclusions for the SAS-technology. Regarding materials and experimental setups we therefore refer to some of our previous publications and one additional manuscript within the current conference proceedings [4-6]. Additionally we report about spatially highly resolved high speed measurements, which were beneficial to calculate time scales of mixing and precipitation.

MATERIALS AND METHODS

Figure 1 indicates the flow sheet of the SAS-plant. A solution of a solute (paracetamol) and an organic solvent (ethanol) is injected into a supercritical antisolvent (CO_2). As the solute is quasi immiscible in the solvent/antisolvent mixture, solute particles are precipitated. Figure 2 shows a drawing of the optically accessible SAS-chamber. The chamber is equipped with three windows (bore diameter of 20 mm), two of them line in sight and the third one in perpendicular orientation.

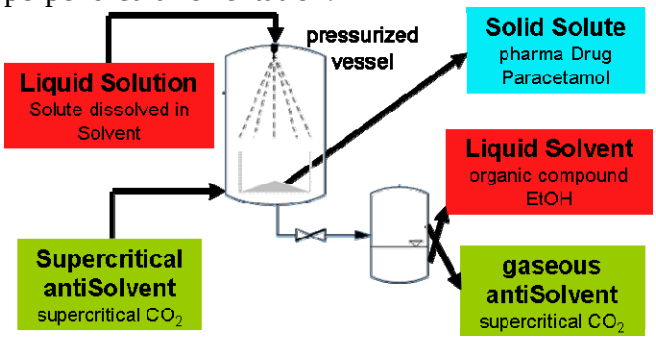

Figure 1: Sketch of the SAS-plant

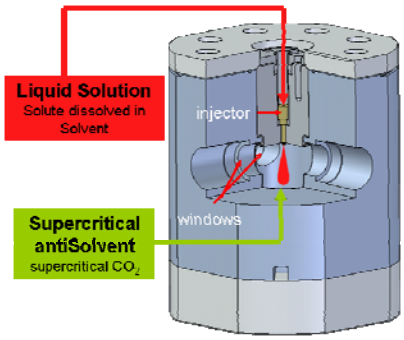

Figure 2: Sketch of the optically accessible pressurized SAS-chamber

The nozzle exit diameter was 100 µm. The solution was injected in a pulsed mode at 1 Hz. The duration of one injection was 1.5 ms. With this pulsed strategy, the amount of solution injected into the antisolvent is negligible. Thus, for batch operation even after 1000 injections, the overall composition inside the SAS-chamber can be assumed to be pure antisolvent. The injection pressure was 20 MPa, while the chamber pressure was 10 MPa. The temperature was set to 313 K, assuring operation conditions above the mixture critical point of the pseudo binary (without solute) system. Considering all experiments described within this manuscript, these process conditions were kept constant. Only the solute concentration in the organic solvent was varied to 0, 3 and 5 weight % paracetamol in ethanol.

Shadography experiments in combination with elastic light scattering experiments were carried out to analyze the intermediate steps taking place inside the SAS-chamber. As can be seen in Figure 3 a long distance microscope in combination with a high speed camera was used. Thus the acquisition of spatially highly resolved images at very high recording rates –up to 100 kHz- is possible, which allows to follow the evolution of the mixing mechanisms. For illumination a high power 250 W halogen lamp was used.

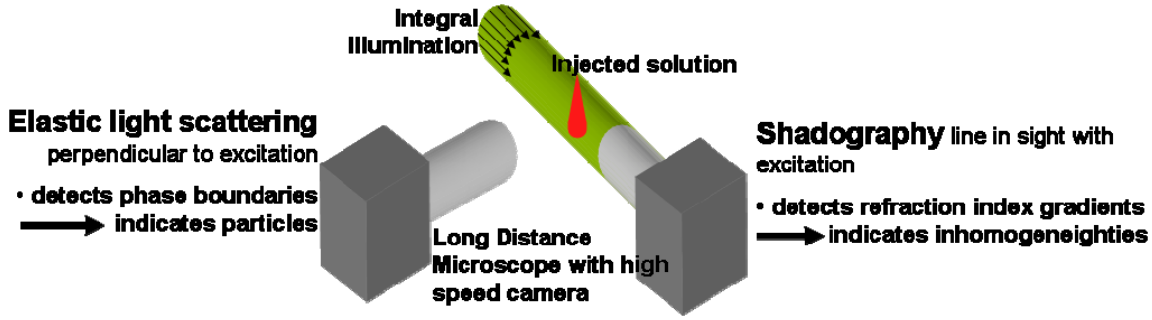

Figure 3: Sketch of the combined shadography and elastic light scattering setup. Only the injected solution is indicated, not the SAS-chamber, which circumvents the injected solution.

Whenever there are phase boundaries within the integral illumination path, light is scattered away from its original path. As some light is scattered perpendicularly, the presence of phase

boundaries –droplets or particles- can be detected with the elastic light scattering technique. In contrast to this, the shadography technique is sensitive towards gradients of the refractive index. Refractive index gradients may change the original path of incident light at small angles. Therefore, the long distance microscope and the high speed camera have to be orientated line in sight with the integral illumination path. As the refractive index is a function of the mixture composition, mixture inhomogenighties can be detected with the shadography technique. The elastic light scattering and shadography experiments were carried out consecutively, and not simultaneously.

A more complex experimental setup was used to measure the mixture composition distribution, the antisolvent partial density distribution and the locations, where particle precipitation starts. As we aimed to receive quantitative information about these mixing mechanisms, we had to identify an optical measurement technique, which signal intensity is on the one hand directly proportional to the number density of solvent or antisolvent molecules and on the other hand species selective. Raman scattering is known to exactly meet these demands. A detailed explanation regarding the Raman imaging setup and some fundamentals on Raman scattering are given within the current conference proceedings by Dowy et al. [6].

RESULTS

Figure 4 shows the shadography (SG) and the elastic light scattering (ELS) measurements for three solute concentrations, 0, 3 and 5 weight % paracetamol in ethanol.

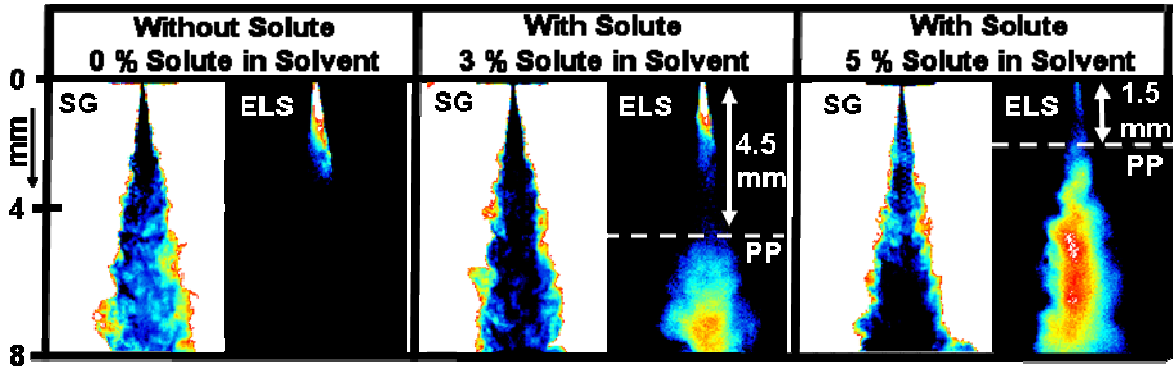

Figure 4: Comparison of shadography (SG) and elastic light scattering (ELS) images for three different solute concentrations. The dashed lines indicate the beginning of particle precipitation.

The bright (white) areas in the SG-images represent homogeneous regions, where the illumination light passed the chamber without being diffracted at refractive index gradients. As refractive index gradients must be assigned to inhomogenities of the mixture composition, the non-white areas indicate the projection image of that part of the injected jet, which is not yet homogenously mixed.

The bright areas in the ELS-images represent regions, where phase boundaries are detected. This may be due to the interfacial tension between the injected solution and the antisolvent close to the injection nozzle and due to the phase boundaries of particles in a certain distance from the injection nozzle. With increasing distance from the injection nozzle, the interfacial tension decreases, until no more ELS-signals can be detected. Further downstream, where particle precipitation (PP) takes place, ELS-signals are detectable again. The ELS-images show, that precipitation can be accelerated, if the solute concentration is increased. This can only be true, if mixing is not significantly faster than nucleation. This means, that having reached supersaturation, particles are formed. The higher the original solute concentration, the

less mixing time is required to reach supersaturation. If mixing was significantly faster than nucleation, the beginning of particle precipitation would not be affected by the solute concentration. Additionally the structures within the SG-images proof, that even 8 mm downstream of the injection nozzle, there are still inhomogenities within the jet. This also shows that mixing time scales are rather long.
To calculate exact values of the respective time scales, one has to know the residence time of an injected fluid element. As we know the particle precipitation distance downstream of the injection nozzle, we can calculate the residence time via the flow field within the jet. For flow sheet calculations the SG-acquisition of the jet at very high recording rates is required. Then one can follow the temporal evolution of the jet structures and calculate the flow field via an optical flow algorithm. Figure 5 shows SG-images which were acquired with a temporal delay of 20 µs and the corresponding flow field which was calculated from these images.

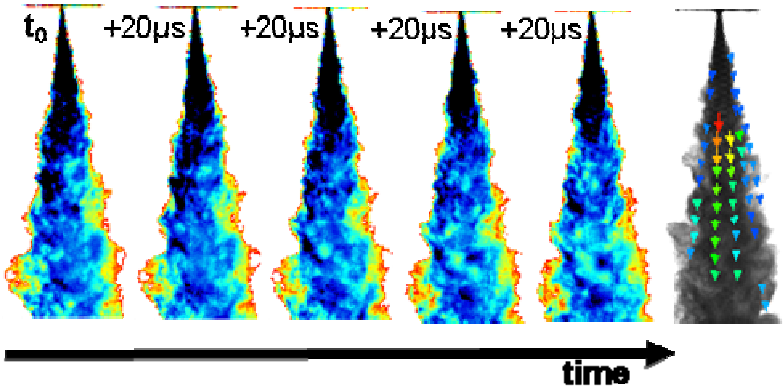

Figure 5: Shadography images of the injected jet and the corresponding flow field image, which was calculated via an optical flow algorithm. The recording rate of image acquisition was 50 kHz.

Assuming, that one injected fluid element moves vertically from the injection nozzle to the dashed white line in Figure 4, which indicates the beginning of precipitation, the time required for this travel is 330 µs and 70 µs for a solute concentration of 3 and 5 weight %, respectively.
Comparing the supersaturation at locations where particle precipitation begins for both solute concentrations, a more precise conclusion on the time scales of mixing and of nucleation can be drawn. Only if the supersaturation at the beginning of nucleation is the same for both original solute concentrations, nucleation must have been much faster than mixing. To check, this, the antisolvent mole fraction x_{CO2} distributions (mean images), which resulted from the Raman-measurements, have to be analyzed. The corresponding mole fraction distributions x_{CO2} of the antisolvent CO_2 are given in Figure 6. The mean images were calculated from 50 single-shot images.
Although the solute molecules were neglected for the antisolvent mole fraction measurements, we define the solute mole fraction to be directly proportional to the solvent mole fraction $x_{Solvent}$.

$$x_{Solute} \propto x_{Solvent} = (1 - x_{CO2}). \quad (1)$$

For the injection of the 3 % solution the antisolvent mole fraction is between 0.95 and 0.96 at the position 4.5 mm downstream of the injector where particle precipitation begins. For the injection of the 5 % solution the antisolvent mole fraction is between 0.92 and 0.93 at the position 1.5 mm downstream of the injector where particle precipitation begins. Thus, the solvent mole fraction $x_{Solvent}$ is about 0.045 and 0.075 for the injection of the 3 % and 5 % solution, respectively. As the solvent mole fraction ratio 0.075/0.045 at the beginning of

particle precipitation is exactly the ratio of the original solute concentrations 5/3, the nucleation time can be assumed to be much smaller than time required to reach supersaturation.

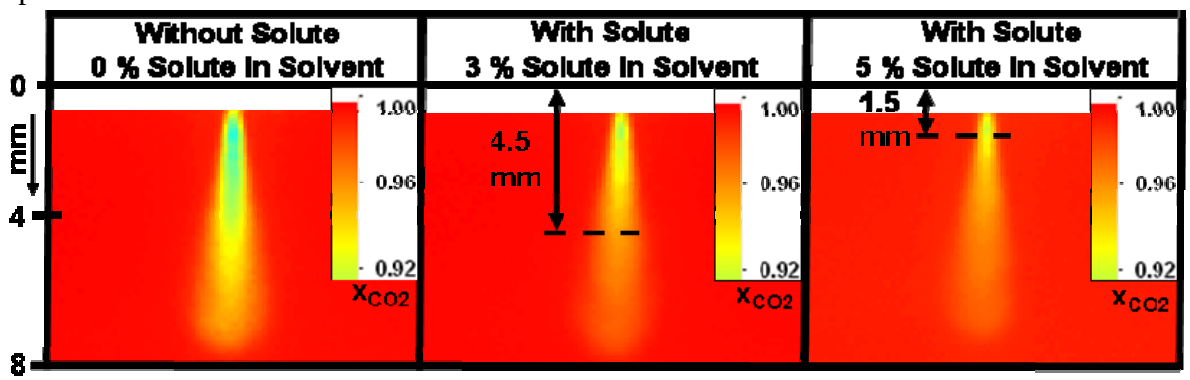

Figure 6: Mole fraction distribution x_{CO2} of the antisolvent CO_2 at different solute concentrations. The locations of particle precipitation beginning, which were identified in Figure 4 are indicated as dashed lines.

Figure 6 also shows that the original solute concentration affects the mixture generation process in an unexpected way. The higher the solute concentration, the higher are the antisolvent mole fractions x_{CO2}. As the amount of solution injected into the antisolvent is equal for the three solute concentrations, this result must be explained by faster mixing mechanisms at higher solute concentrations. These differences in mixing velocities must be ascribed to different phase behaviours of the system paracetamol, ethanol and CO_2 at different solute concentrations. To proof this, Raman scattering was used to image the partial density distribution of the antisolvent. The corresponding partial density distributions of CO_2 are illustrated in Figure 7.

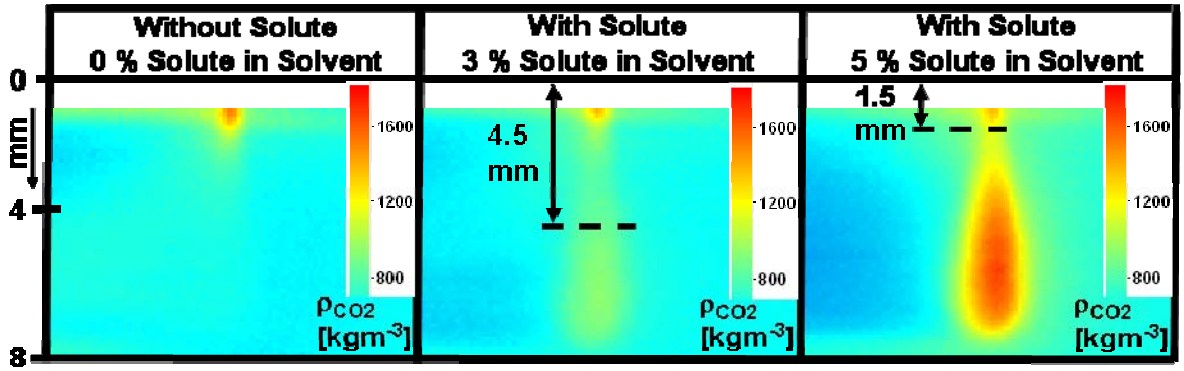

Figure 7: Partial density distribution of the antisolvent CO_2 at different solute concentrations. The locations of particle precipitation beginning, which were identified in Figure 4 are indicated as dashed lines.

Figure 7 shows, that the partial density of the antisolvent CO_2 inside the jet is higher than in the surrounding bulk, if a solution of solute and solvent is injected. For the injection of the 5 % solution a partial density increase of approximately 3 was identified. Partial density increases of this magnitude are only known for mixtures of ethanol and CO_2 below the mixture critical point. Throughout all our experiments, the process conditions were set to exceed the mixture critical point of the pseudo binary (without solute) mixture. Therefore we conclude that the solvent paracetamol has a big impact onto the phase behaviour during the mixture process. From Figure 7 it is evident, that not alone the presence of the paracetamol but its concentration affects the phase behaviour. This may be the reason, why for the system paracetamol, ethanol and CO_2 amorphous nano-particles were never produced [7-10].

CONCLUSION

Optical measurement techniques are a beneficial tool to analyze and finally understand the functioning chain of the SAS particle precipitation. As the optical measurements can be carried out with a high temporal and spatial resolution, they qualify to resolve fast mechanisms on a small scale. Adoption of optical techniques to other supercritical technologies would provide a deeper insight into the respective mechanisms.

ACKNOWLEDGEMENT

The authors gratefully acknowledge funding of parts of this work by the German National Science Foundation (DFG) and funding of the Erlangen Graduate School in Advanced Optical Technologies (SAOT) by the DFG in the framework of the excellence initiative.

REFERENCES:

1. J. Baldyga, M. Henczka, and B. Y. Shekunov, "Fluid dynamics, mass transfer, and particle formation in supercritical fluids," in *Supercritical Fluid Technology for Drug Product Development*, P. York, U. B. Kompella, and B. Y. Shekunov, eds. (Marcel Dekker, Inc., Bradford, **2004**), pp. 91–157.
2. E. Reverchon, G. Caputo, and I. De Marco, "Role of Phase Behavior and Atomization in the Supercritical Antisolvent Precipitation," J. Supercrit. Fluids 42, 6406-6414 **(2003)**.
3. E. Reverchon, I. De Marco, and E. Torino, "Nanoparticles production by supercritical antisolvent precipitation: A general interpretation," J. Supercrit. Fluids 43, 126-138 **(2007)**.
4. S. Dowy, A. Braeuer, and A. Leipertz, "CO2 partial density distribution under dynamic mixture generation conditions in the supercritical antisolvent process," in *11th European Meeting on Supercritical Fluids*, (ISASF, **2008**), 113.
5. S. Dowy, A. Braeuer, R. Schatz, E. Schluecker, and A. Leipertz, "CO2 partial density distribution during high-pressure mixing with ethanol in the supercritical antisolvent process," J. Supercrit. Fluids In Press, Corrected Proof, doi:10.1016/j.supflu.2008.1010.1017 **(2009)**.
6. S. Dowy, A. Braeuer, R. Schatz, E. Schluecker, and A. Leipertz, "Particle Nucleation and Mixture Formation Characterized by a combination of Raman and Mie Scattering," in *9th international Symposium on Supercritical Fluids*, (ISASF, **2009**),
7. S. Bristow, T. Shekunov, B. Y. Shekunov, and P. York, "Analysis of the supersaturation and precipitation process with supercritical CO_2," J. Supercrit. Fluids 21, 257-271 **(2001)**.
8. B. Y. Shekunov, J. Baldyga, and P. York, "Particle formation by mixing with supercritical antisolvent at high Reynolds numbers," Chem. Eng. Sci. 56, 2421-2433 **(2001)**.
9. B. Y. Shekunov, M. Hanna, and P. York, "Crystallization process in turbulent supercritical flows," J Cryst. Growth 198/199, 1345-1351 **(1999)**.
10. B. Y. Shekunov and P. York, "Crystallization processes in pharmaceutical technology and drug delivery design," J. of Cryst. Growth 211, 122-136 **(2000)**.